AD-A042 902 AEROSPACE CORP EL SEGUNDO CALIF AEROPHYSICS LAB F/G 11/4
LAMB'S PROBLEM FOR AN IMPULSIVE LINE LOAD ON A LAMINATED COMPOS--ETC(U)
JUN 77 C SVE, J MIKLOWITZ F04701-76-C-0077
UNCLASSIFIED TR-0077(2240)-2 SAMSO-TR-77-129 NL

1 OF 1
ADA042902

END
DATE FILMED
9-77
DDC

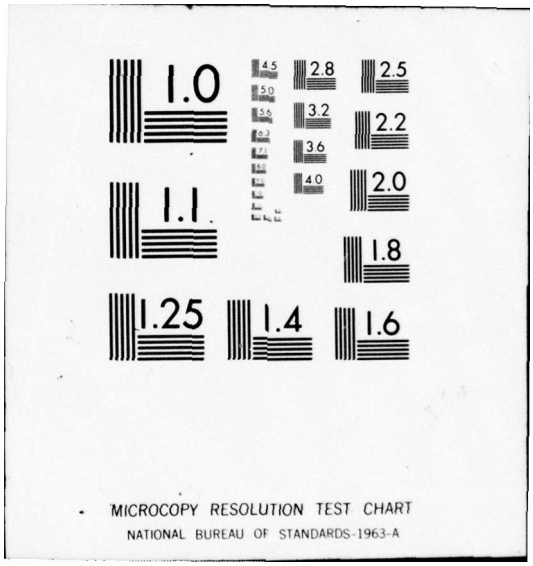
1.0
1.1
1.25
1.4
1.6
1.8
2.0
2.2
2.5
2.8
3.2
3.6
4.0
4.5
5.0
5.6
6.3
7.1
MICROCOPY RESOLUTION TEST CHART
NATIONAL BUREAU OF STANDARDS-1963-A

REPORT SAMSO-TR-77-129

Lamb's Problem for an Impulsive Line Load on a Laminated Composite

Aerophysics Laboratory
The Ivan A. Getting Laboratories
The Aerospace Corporation
El Segundo, Calif. 90245

30 June 1977

Interim Report

Prepared for
SPACE AND MISSILE SYSTEMS ORGANIZATION
AIR FORCE SYSTEMS COMMAND
Los Angeles Air Force Station
P.O. Box 92960, Worldway Postal Center
Los Angeles, Calif. 90009

This interim report was submitted by The Aerospace Corporation, El Segundo, CA 90245, under Contract No. F04701-76-C-0077 with the Space and Missile Systems Organization, Deputy for Advanced Space Programs, P.O. Box 92960, Worldway Postal Center, Los Angeles, CA 90009. It was reviewed and approved for The Aerospace Corporation by W. R. Warren, Jr., Director, Aerophysics Laboratory. Lieutenant Dara Batki, SAMSO/YAPT, was the project officer for Advanced Space Programs.

This report has been reviewed by the Information Office (OI) and is releasable to the National Technical Information Service (NTIS). At NTIS, it will be available to the general public, including foreign nations.

This technical report has been reviewed and is approved for publication. Publication of this report does not constitute Air Force approval of the report's findings or conclusions. It is published only for the exchange and stimulation of ideas.

Dara Batki

Dara Batki, Lt, USAF
Project Officer

J Gassmann

Joseph Gassmann, Major, USAF

FOR THE COMMANDER

Leonard E. Baltzell

LEONARD E. BALTZELL, Col, USAF, Asst.
Deputy for Advanced Space Programs

UNCLASSIFIED

SECURITY CLASSIFICATION OF THIS PAGE (When Data Entered)

REPORT DOCUMENTATION PAGE

READ INSTRUCTIONS BEFORE COMPLETING FORM

1. REPORT NUMBER: SAMSO-TR-77-129	2. GOVT ACCESSION NO.
3. RECIPIENT'S CATALOG NUMBER	
4. TITLE (and Subtitle): LAMB'S PROBLEM FOR AN IMPULSIVE LINE LOAD ON A LAMINATED COMPOSITE.	5. TYPE OF REPORT & PERIOD COVERED: Interim Rept.
	6. PERFORMING ORG. REPORT NUMBER: TR-0077(2240)-2
7. AUTHOR(s): Charles Sve and Julius Miklowitz (Consultant)	8. CONTRACT OR GRANT NUMBER(s): F04701-76-C-0077
9. PERFORMING ORGANIZATION NAME AND ADDRESS: The Aerospace Corporation, El Segundo, Calif. 90245	10. PROGRAM ELEMENT, PROJECT, TASK AREA & WORK UNIT NUMBERS
11. CONTROLLING OFFICE NAME AND ADDRESS: Space and Missile Systems Organization, Air Force Systems Command, Los Angeles, Calif. 90009	12. REPORT DATE: 30 June 1977 13. NUMBER OF PAGES: 53
14. MONITORING AGENCY NAME & ADDRESS (if different from Controlling Office): 57p.	15. SECURITY CLASS. (of this report): Unclassified 15a. DECLASSIFICATION/DOWNGRADING SCHEDULE

16. DISTRIBUTION STATEMENT (of this Report)

Approved for public release; distribution unlimited.

17. DISTRIBUTION STATEMENT (of the abstract entered in Block 20, if different from Report)

18. SUPPLEMENTARY NOTES

19. KEY WORDS (Continue on reverse side if necessary and identify by block number)

Wave Propagation
Composite Materials
Geometric Dispersion

20. ABSTRACT (Continue on reverse side if necessary and identify by block number)

The effective stiffness theory developed by Sun, Achenbach, and Herrmann is used to model a periodically laminated linearly elastic half space that is subjected to an impulsively applied line load. The laminations are parallel to the free surface. An approximate solution is constructed by approximating formal solutions (inversion integrals) near saddle points for low frequency and large distance from the source. Contributions include the responses of the body waves as well as the head and Rayleigh waves. Numerical results

DD FORM 1473 (FACSIMILE)

UNCLASSIFIED

SECURITY CLASSIFICATION OF THIS PAGE (When Data Entered)

409367

19. KEY WORDS (Continued)

20. ABSTRACT (Continued)

are presented in order to illustrate the differences between the dispersive and nondispersive solutions.

PREFACE

The authors are grateful to Mary Ellen Brennan for her patience and very competent numerical evaluations during this investigation.

CONTENTS

TABLE

FIGURES

I. INTRODUCTION

Lamb's [1] half space problems have been the subject of many investigations because they are fundamental to numerous two-dimensional applications. Kraut [2] extended Lamb's solution for a line source on an isotropic half space to a transversely isotropic half space by developing a solution with the Cagniard-deHoop technique. A summary of this solution and a list of related references are available in Kraut's review article [3]. Kraut's solution is the nondispersive solution to the present problem corresponding to a replacement of the laminated composite with a homogeneous transversely isotropic material.

In order to construct a solution that includes the effect of geometrical dispersion, we begin with the equations of motion and boundary conditions from the effective stiffness theory advanced by Sun, Achenbach, and Herrmann [4]. One of several other approximate theories that are available for composites could have been selected for this study; however, the form of the fundamental solutions obtained here would not be changed by such a choice. Two related problems that demonstrated the effect of geometrical dispersion on the dynamic response of a laminated composite have recently been solved [5, 6] within the context of this effective stiffness theory, and those solutions provide the background for this investigation. The first problem [5] was concerned with one-dimensional pulse propagation in an obliquely laminated composite; the second [6] resulted in a steady- tate solution for loads moving over a composite half space. In each case, a far-field solution was developed that contained low-frequency long waves consistent with the basic assumptions in the effective stiffness theory. A near-field solution would require high-frequency short wave information that is available only from the exact theory. In other words, the approximations that were used to construct the solutions matched the approximations inherent in the field equations and boundary conditions of the effective stiffness theory. The same approach is followed in the present work.

In the following analysis, Fourier and Laplace transforms are used to obtain a formal solution to the problem. A far-field solution is developed for the body wave responses in the interior of the half space by first using the method of steepest descents to approximate the inversion integrals near the appropriate saddle points. Then, the phase velocities are expanded for low frequency, which permits the inversion of the Laplace transforms. The head wave and Rayleigh wave are treated in a similar manner.

The final results show that from two to five separate waves contribute to the response, depending on the location of the observer in the laminated half space. The quasi-dilatational wave and head wave are shown to be one-sided waves, whereas the quasi-equivoluminal wave is one-sided until a critical angle is exceeded, and then it becomes two-sided. Also, cusps may develop on the quasi-equivoluminal wave. Geometric dispersion caused by the laminations is shown to strongly influence the body wave results by eliminating the singular behavior that exists for the displacements at the wavefronts in the nondispersive solution. The singularity in the Rayleigh surface wave is also found to be eliminated by geometric dispersion.

II. STATEMENT OF PROBLEM

The periodically laminated half space subjected to the line impulse $P_0\delta(t)\delta(x_1)$ is shown in Fig. 1. P_0 is the magnitude of the line impulse; $\delta(t)$ and $\delta(x_1)$ represent Dirac delta functions with arguments time t and spatial coordinate x_1. Because the half space is in a state of plane strain, the equations of motion from the effective stiffness theory [4] can be written as

$$-a_1\partial_{1122}u_1 + a_2\partial_{11}u_1 + a_3\partial_{22}u_1 + a_4\partial_{12}u_2 + a_5\partial_{112}\psi_{21}$$
$$-a_6\partial_2\psi_{21} + a_7\partial_1\psi_{22} = -b_1\partial_{22}\ddot{u}_1 + b_2\ddot{u}_1 + b_3\partial_2\ddot{\psi}_{21} \tag{1}$$

$$-a_8\partial_{1122}u_2 + a_9\partial_{11}u_2 + a_{10}\partial_{22}u_2 + a_4\partial_{12}u_1 + a_{11}\partial_1\psi_{21}$$
$$+ a_{12}\partial_{112}\psi_{22} - a_{13}\partial_2\psi_{22} = -b_1\partial_{22}\ddot{u}_2 + b_2\ddot{u}_2 + b_3\partial_2\ddot{\psi}_{22} \tag{2}$$

$$a_5\partial_{112}u_1 - a_6\partial_2u_1 + a_{11}\partial_1u_2 - a_{14}\partial_{11}\psi_{21} + a_{15}\psi_{21}$$
$$= b_3\partial_2\ddot{u}_1 - b_4\ddot{\psi}_{21} \tag{3}$$

$$a_{12}\partial_{112}u_2 - a_{13}\partial_2u_2 + a_7\partial_1u_1 - a_{16}\partial_{11}\psi_{22} + a_{17}\psi_{22}$$
$$= b_3\partial_2\ddot{u}_2 - b_4\ddot{\psi}_{22} \tag{4}$$

where u_1 and u_2 are the average displacements in the x_1 and x_2 directions, respectively, and ψ_{21} and ψ_{22} are microdeformations in the stiff laminations. The notation $\partial_i u_j = \partial u_j/\partial x_i$ is used, and dots above variables denote partial differentiation with respect to time. The constants in the above equations of motion are defined as follows:

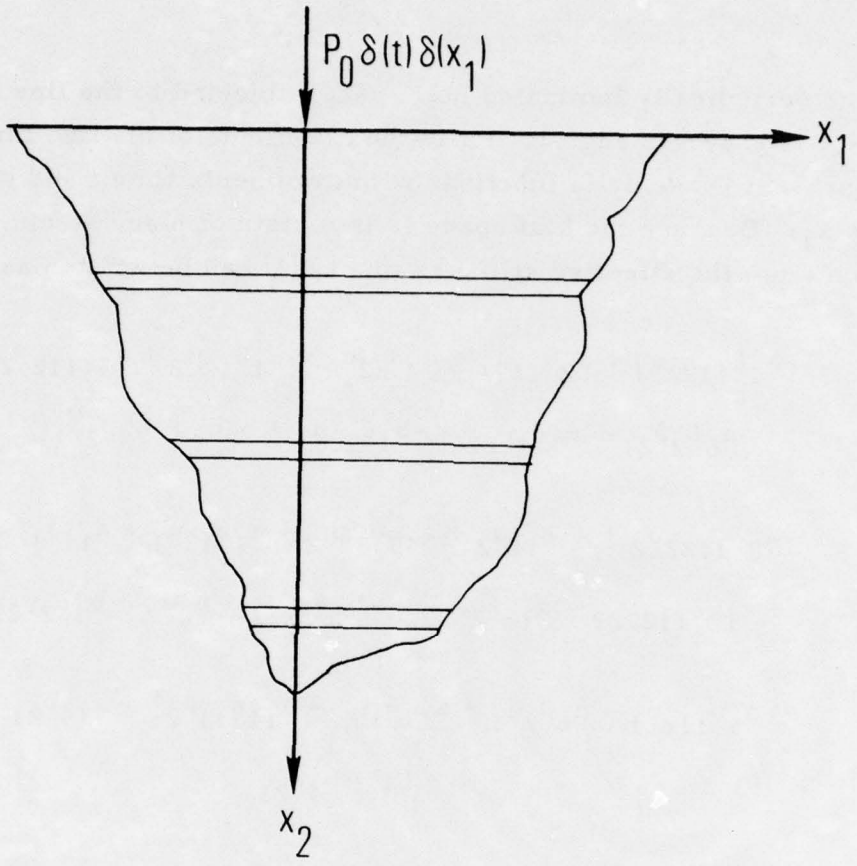

Figure 1. Laminated Half Space with Line Impulse

$$a_1 = \frac{d_m^2}{12}(\lambda_m + 2\mu_m)/(1 - \eta)$$

$$a_2 = \eta(\lambda_f + 2\mu_f) + (1 - \eta)(\lambda_m + 2\mu_m)$$

$$a_3 = \mu_m/(1 - \eta)$$

$$a_4 = \lambda_m + \mu_m$$

$$a_5 = \eta a_1$$

$$a_6 = \eta a_3$$

$$a_7 = \eta(\lambda_f - \lambda_m)$$

$$a_8 = d_m^2 a_3/12$$

$$a_9 = \eta\mu_f + (1 - \eta)\mu_m$$

$$a_{10} = (\lambda_m + 2\mu_m)/(1 - \eta)$$

$$a_{11} = \eta(\mu_f - \mu_m)$$

$$a_{12} = \eta a_8$$

$$a_{13} = \eta a_{10}$$

$$a_{14} = d_f^2 a_2/12$$

$$a_{15} = \eta[(1 - \eta)\mu_f + \eta\mu_m]/(1 - \eta)$$

$$a_{16} = d_f^2 a_9/12$$

$$a_{17} = \eta[(1 - \eta)(\lambda_f + 2\mu_f) + \eta(\lambda_m + 2\mu_m)]/(1 - \eta) \qquad (5)\ (\text{Cont.})$$

$$b_1 = \rho_m \frac{d_m^2}{12}/(1 - \eta)$$

$$b_2 = \eta\rho_f + (1 - \eta)\rho_m$$

$$b_3 = \eta b_1$$

$$b_4 = d_f^2 b_2/12 \tag{5}$$

where

$$\eta = d_f/h \quad , \quad h = d_f + d_m \, . \tag{6}$$

The preceding definitions depend on the Lamé parameters, thicknesses, and densities of the soft (m) and stiff (f) laminations, which are denoted by λ_m, μ_m, d_m, and ρ_m and λ_f, μ_f, d_f, and ρ_f, respectively.

The half space is initially at rest, i.e., u_1, u_2, $\dot{u}_1$, $\dot{u}_2$, ψ_{22} ... vanish at $t = 0$, and the tractions on the surface are specified as

$$t_1 = 0 \tag{7}$$

and

$$t_2 = -P_0 \delta(x_1)\delta(t) \tag{8}$$

where t_1 and t_2 are shear and normal tractions, respectively. It is also required that all displacements and stresses vanish at an infinite distance from the load.

III. FORMAL SOLUTION OF PROBLEM

In order to develop a formal solution to this problem, an exponential Fourier transform defined as

$$\tilde{f}(\kappa) = \int_{-\infty}^{\infty} f(x_1) \exp(i\kappa x_1) dx_1 \tag{9}$$

with inverse

$$f(x_1) = \frac{1}{2\pi} \int_{-\infty}^{\infty} \tilde{f}(\kappa) \exp(-i\kappa x_1) d\kappa \tag{10}$$

and a Laplace transform defined as

$$\bar{f}(\sigma) = \int_{0}^{\infty} f(t) \exp(-\sigma t) dt \tag{11}$$

with inverse

$$f(t) = \frac{1}{2\pi i} \int_{Br_1} \bar{f}(\sigma) \exp(\sigma t) d\sigma \tag{12}$$

are applied to equations (1)-(4) subject to the quiescent initial conditions. Nondimensional parameters are then introduced, and the resulting set of equations is reduced to

$$B_1 \frac{d^2\tilde{\bar{u}}}{dy^2} - isB_3 \frac{d\tilde{\bar{v}}}{dy} - s^2 B_2 \tilde{\bar{u}} = 0 \tag{13}$$

and

$$B_4 \frac{d^2\tilde{\bar{v}}}{dy^2} - isB_3 \frac{d\tilde{\bar{u}}}{dy} - s^2 B_5 \tilde{\bar{v}} = 0 \tag{14}$$

where nondimensional quantities are defined as

$$u = u_1/h \quad , \quad v = u_2/h \quad , \quad x = x_1/h \quad , \quad y = x_2/h \tag{15}$$

$$\tau = t(\mu_m/\rho_m)^{1/2}/h \quad , \quad \xi = \kappa h \quad , \quad s = \sigma h/(\mu_m/\rho_m)^{1/2} . \tag{16}$$

The coefficients in equations (13) and (14) are given by

$$\begin{aligned} B_1 &= A_1 - A_4^2/A_{10} \\ B_2 &= A_2 - A_5^2/A_{11} \\ B_3 &= A_3 + A_5A_9/A_{11} + A_4A_8/A_{10} \\ B_4 &= A_6 - A_9^2/A_{11} \\ B_5 &= A_7 - A_8^2/A_{10} \end{aligned} \tag{17}$$

where

$$\begin{aligned} A_1 &= (1 + q^2\delta_m)(1 - \eta)s^2/12 + 1/(1 - \eta) \\ A_2 &= (\eta\theta + 1 - \eta) + [\eta\gamma\delta_f + (1 - \eta)\delta_m]q^2 \\ A_3 &= (\epsilon_m + 1)q \\ A_4 &= \eta A_1 \\ A_5 &= \eta(\epsilon_f\gamma - \epsilon_m)q \end{aligned} \tag{18 (Cont.)}$$

$$A_6 = \delta_m/(1 - \eta) + (q^2 + 1)(1 - \eta)s^2/12$$

$$A_7 = (\eta\theta + 1 - \eta) + (\eta\gamma + 1 - \eta)q^2$$

$$A_8 = \eta(\gamma - 1)q$$

$$A_9 = \eta A_6$$

$$A_{10} = s^2\eta^2 A_2/12 + \eta\gamma + \eta^2/(1 - \eta)$$

$$A_{11} = s^2\eta^2 A_7/12 + \eta\gamma\delta_f + \eta^2\delta_m/(1 - \eta) \qquad (18)$$

and

$$\gamma = \mu_f/\mu_m \quad , \quad \theta = \rho_f/\rho_m$$

$$\delta_f = \epsilon_f + 2 = (\lambda_f + 2\mu_f)/\mu_f$$

$$\delta_m = \epsilon_m + 2 = (\lambda_m + 2\mu_m)/\mu_m . \qquad (19)$$

Also, in anticipation of the form of the final solution, ξ has been eliminated by substitution of a nondimensional slowness defined as

$$q = \xi/s . \qquad (20)$$

Note that s is confined to the dispersive terms (those terms that contain the number 12) in the definitions for the A's.

Equations (13) and (14) are combined to yield

$$B_1B_4 \frac{d^4\tilde{\bar{u}}}{dy^4} - (B_2B_4 + B_1B_5 - B_3^2)\, s^2 \frac{d^2\tilde{\bar{u}}}{dy^2} + B_2B_5 s^4 \tilde{\bar{u}} = 0 . \qquad (21)$$

Then, because the general solution of equation (21) is proportional to exp(-msy), we obtain

$$\Phi(m, q, s) = m^4 B_1 B_4 - (B_2 B_4 + B_1 B_5 - B_3^2) m^2 + B_2 B_5 = 0. \qquad (22)$$

Since $y \geq 0$ and s can be considered positive, we choose the two roots of this equation that have positive real parts in order to satisfy the conditions at infinity ($y \to \infty$). The transformed displacements and microdeformations then become

$$\begin{aligned} \tilde{u} &= C_1 e_1 + C_2 e_2 \\ \tilde{v} &= C_1 D_1 e_1 + C_2 D_2 e_2 \\ \tilde{\psi}_{21} &= C_1 E_1 e_1 + C_2 E_2 e_2 \\ \tilde{\psi}_{22} &= C_1 F_1 e_1 + C_2 F_2 e_2 \end{aligned} \qquad (23)$$

where

$$e_j = \exp(-m_j sy) \quad , \quad j = 1, 2 \qquad (24)$$

and C_1 and C_2 are arbitrary constants to be determined from the boundary conditions. The other coefficients in equation (23) are defined as

$$\begin{aligned} D_j &= (B_2 - B_1 m_j^2)/i m_j B_3 \\ E_j &= s(iA_8 D_j - m_j A_4)/A_{10} \\ F_j &= s(iA_5 - m_j D_j A_9)/A_{11} \quad , \quad j = 1, 2 . \end{aligned} \qquad (25)$$

Expressions for the two tractions are available [7] and their transforms reduce to

$$\tilde{t}_1/\mu_m = C_1 G_1 e_1 + C_2 G_2 e_2 \tag{26}$$

$$\tilde{t}_2/\mu_m = C_1 H_1 e_1 + C_2 H_2 e_2 \tag{27}$$

where

$$\begin{aligned} G_j &= -iqsD_j - m_j s A_1 - A_4 E_j \\ H_j &= -iqs\,\epsilon_m - m_j s D_j A_6 - A_9 F_j \qquad , \qquad j = 1, 2 \, . \end{aligned} \tag{28}$$

In order to satisfy the boundary conditions specified by equations (7) and (8)

$$C_1 = PG_2/\Delta \tag{29}$$

$$C_2 = -PG_1/\Delta \tag{30}$$

in which

$$\Delta = G_1 H_2 - G_2 H_1 \tag{31}$$

and a nondimensional line impulse is introduced as

$$P = P_0(\mu_m/\rho_m)^{1/2}/\mu_m h^2 \, . \tag{32}$$

Double inversion integrals for the transformed quantities in equation (23) can now be written by using equations (10) and (12). This completes the formal solution to the problem.

IV. FAR-FIELD SOLUTION FOR BODY WAVES

Since an explicit evaluation of the double inversion integrals would be quite complicated, if not impossible, approximations are sought in order to construct a far-field solution. The Laplace-transformed displacements are given by

$$\bar{u}(x, y, s)/P = \frac{1}{2\pi}\int_{-\infty}^{\infty} [G_2 \exp(-iqsx - m_1 sy) - G_1 \exp(-iqsx - m_2 sy)]\Delta^{-1} s\,dq \tag{33}$$

$$\bar{v}(x, y, s)/P = \frac{1}{2\pi}\int_{-\infty}^{\infty} [G_2 D_1 \exp(-iqsx - m_1 sy) - G_1 D_2 \exp(-iqsx - m_2 sy)]\Delta^{-1} s\,dq \quad . \tag{34}$$

We first consider equation (22), which is a polynomial with three variables that provides the roots m_1 and m_2. If s is set to zero, the resulting equation defines the nondispersive two-dimensional slowness surface for a transversely isotropic material in plane strain

$$\Phi_0(m, q) = \Phi(m, q, s)\Big|_{s=0} = 0. \tag{35}$$

This slowness surface is shown in Fig. 2 for $\gamma = 100$, $\eta = 0.8$, $\theta = 3$, $\nu_m = 0.35$, and $\nu_f = 0.3$, where the limiting values are the reciprocals of the wave speeds

$$\beta_{11} = \left\{\frac{[\gamma\delta_f + \eta\delta_m/(1-\eta)][\eta\gamma\delta_f + (1-\eta)\delta_m] - \eta(\gamma\epsilon_f - \epsilon_m)^2}{(1 - \eta + \eta\theta)[\gamma\delta_f + \eta\delta_m/(1-\eta)]}\right\}^{1/2} \tag{36}$$

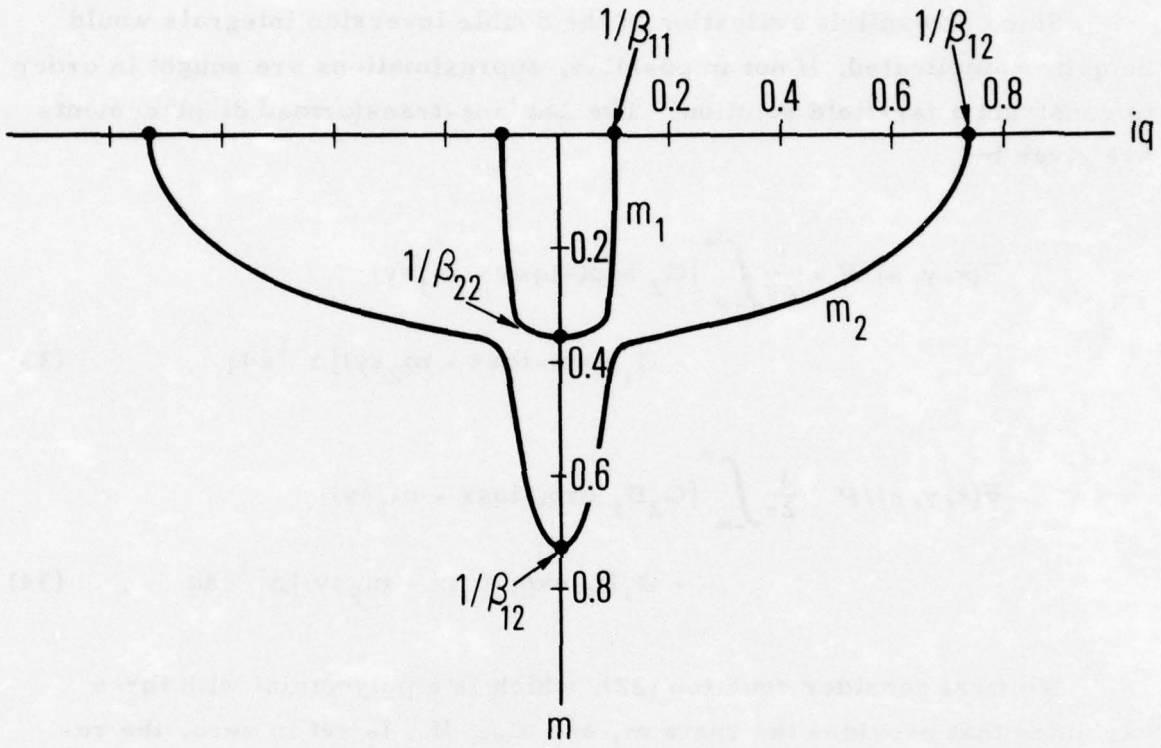

Figure 2. Slowness Surface

$$\beta_{22} = \left\{ \frac{\gamma \delta_m \delta_f}{(1 - \eta + \eta\theta)[(1 - \eta)\gamma\delta_f + \eta\delta_m]} \right\}^{1/2} \tag{37}$$

$$\beta_{12} = \beta_{21} = \left\{ \frac{\gamma}{(1 - \eta + \eta\theta)[\gamma(1 - \eta) + \eta]} \right\}^{1/2} . \tag{38}$$

For the present data, $\beta_{11} = 9.47$, $\beta_{22} = 2.82$, and $\beta_{12} = 1.36$.

Points on the wave surface satisfy

$$iqx + my - \tau = 0 \tag{39}$$

and since a vector from the origin to a point on the wave surface is parallel to the normal to the slowness surface (Fig. 3)

$$x = -iK\Phi_{0,q} \quad , \quad y = K\Phi_{0,m} \tag{40}$$

where K is a constant, and the comma denotes partial differentiation. Substitution of equation (40) into (39) yields

$$K = \tau/(q\Phi_{0,q} + m\Phi_{0,m}) \tag{41}$$

and therefore, from equation (40), the wave surface is defined by

$$x = -i\tau\Phi_{0,q}/(q\Phi_{0,q} + m\Phi_{0,m}) \tag{42}$$

$$y = \tau\Phi_{0,m}/(q\Phi_{0,q} + m\Phi_{0,m}) . \tag{43}$$

In addition, m and q must be on the slowness surface, as given by equation (35). Expressions for the derivatives that appear in equations (42) and (43) are given in Appendix A; the wave surface that corresponds to the slowness surface in Fig. 2 is shown in Fig. 4.

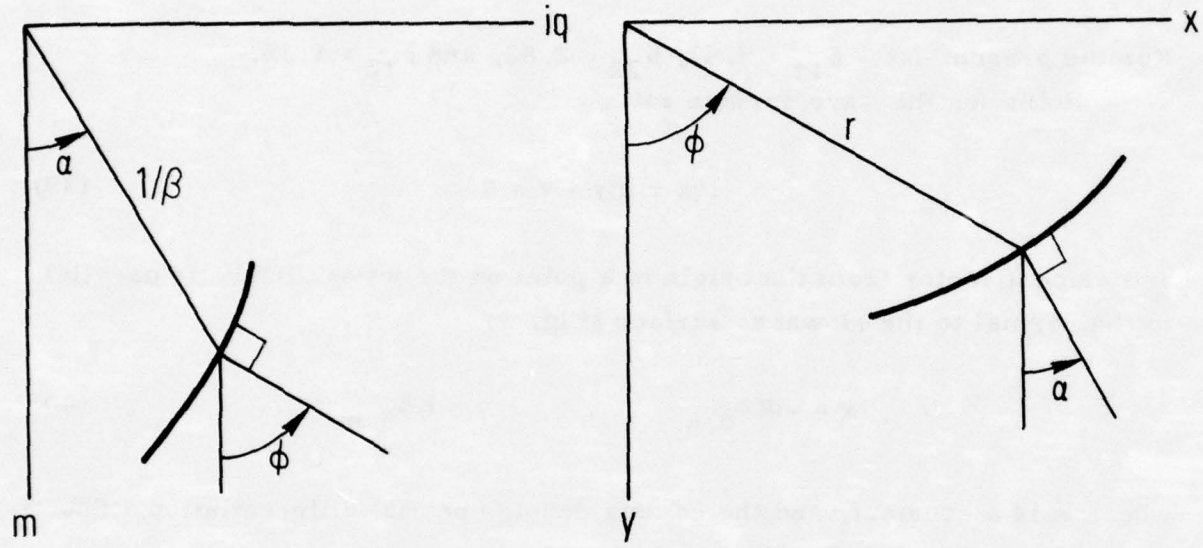

Figure 3. Relationship Between Slowness and Wave Surfaces

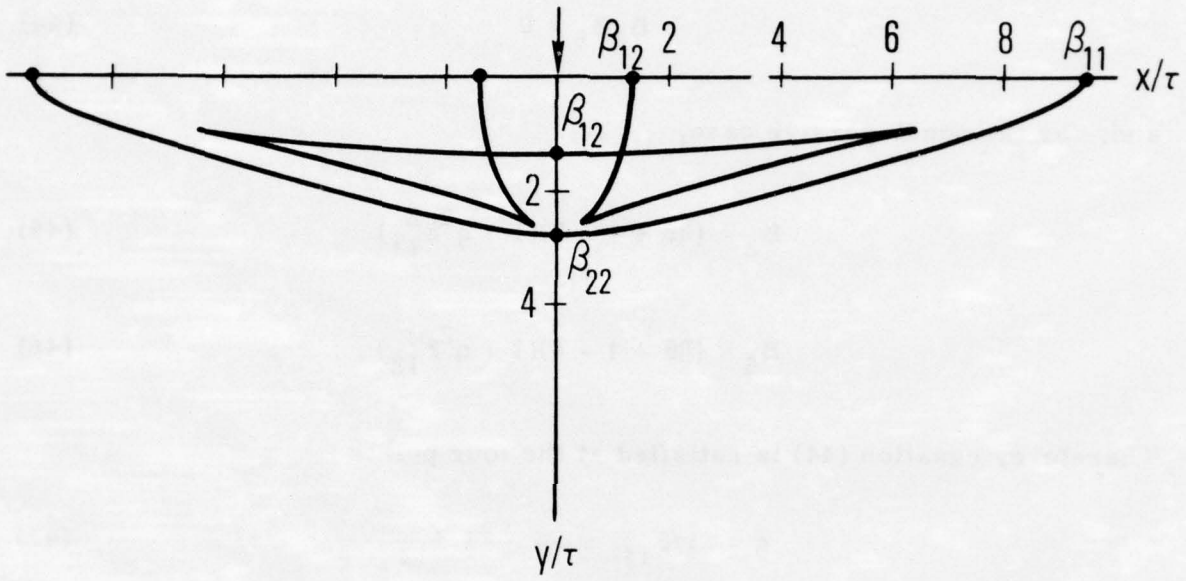

Figure 4. Wave Surface

With the foregoing as background, we return to the evaluation of the integrals in equations (33) and (34). A branch point occurs whenever $m = 0$, which reduces equation (22) to

$$B_2 B_5 = 0 \tag{44}$$

and, for the nondispersive case,

$$B_2 = (\eta\theta + 1 - \eta)(1 + q^2\beta_{11}^2) \tag{45}$$

$$B_5 = (\eta\theta + 1 - \eta)(1 + q^2\beta_{12}^2) . \tag{46}$$

Therefore, equation (44) is satisfied at the four points

$$q = \pm i/\beta_{11} \quad , \quad \pm i/\beta_{12} . \tag{47}$$

Other branch points occur when $m_1 = m_2$, and these can be determined by setting the discriminant of equation (22) to zero. Rayleigh poles ($q = \pm i/\beta_R$) also exist when $\Delta = 0$, [7]. The branch points and Rayleigh pole located in the lower half of the q-plane are shown in Fig. 5. Branch cuts are also indicated in the figure. The path of integration along the real q axis can be replaced with a Cagniard-deHoop path in the lower half of the q-plane for $x > 0$. This problem was solved for the nondispersive case by Kraut [2] and provides the first approximation to the present dispersive problem. Kraut's solution is exact and valid everywhere, including near the wavefronts shown in Fig. 4. He also determined that the displacements were singular at the wavefronts with strength $O(|\tau - \tau^*|^{-1/2})$, whereas, at the cusp tips, the singularity became $O(|\tau - \tau^*|^{-2/3})$, where τ^* corresponds to the arrival time of the wavefront. These singularities are directly related to the order of the corresponding saddle point. In the present analysis, the low-frequency

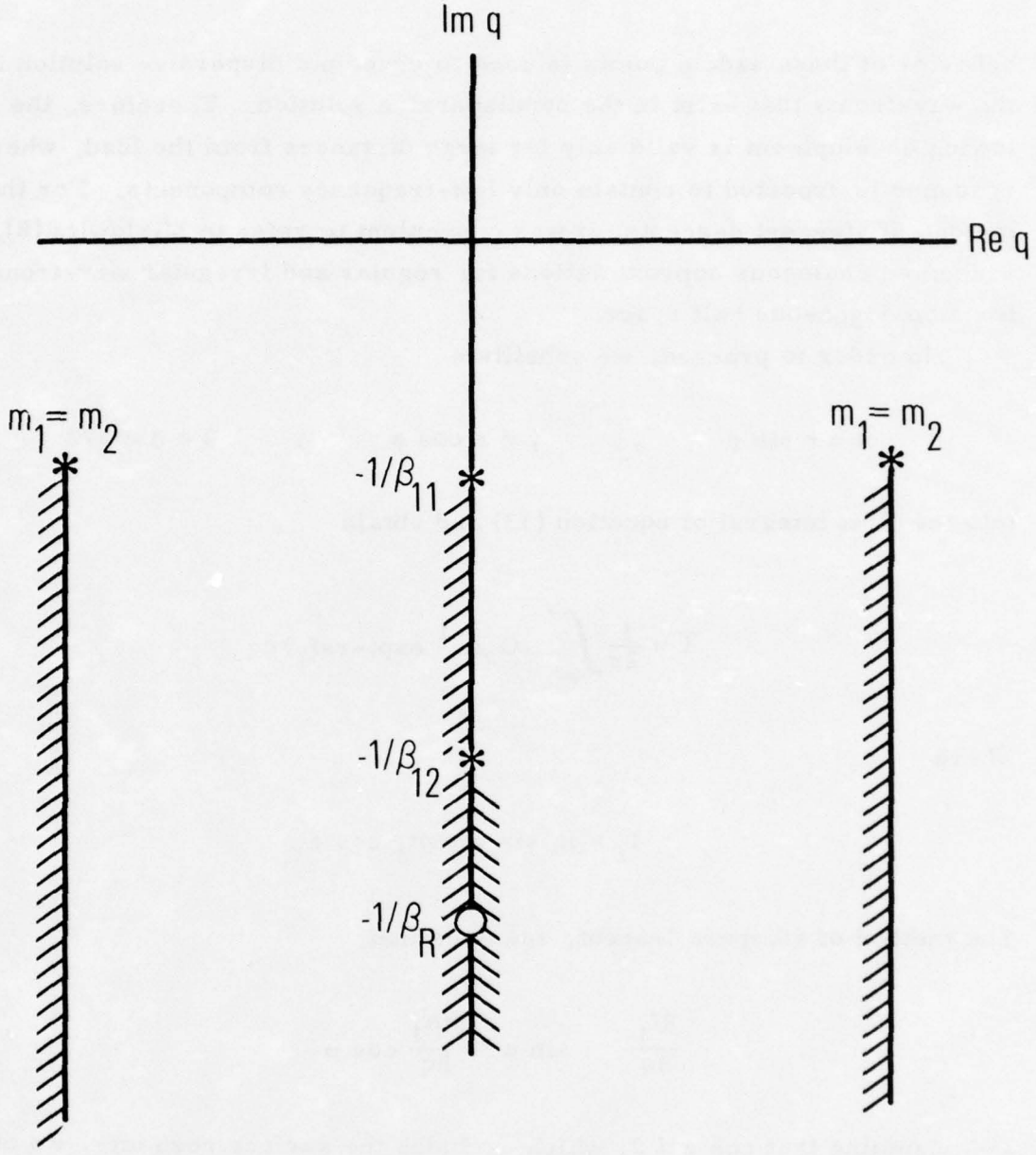

Figure 5. Location of Branch Points and Rayleigh Pole in q-Plane

behavior of these saddle points is used to develop a dispersive solution near the wavefronts that exist in the nondispersive solution. Therefore, the following development is valid only for large distances from the load, where the response is expected to contain only low-frequency components. For the method of steepest descents, it was convenient to refer to Miklowitz [8], who presented analogous approximations for regular and irregular wavefront cases for a homogeneous half space.

In order to proceed, we substitute

$$x = r \sin \phi \quad , \quad y = r \cos \phi \quad , \quad 0 < \phi < \pi/2 \tag{48}$$

into the first integral of equation (33) and obtain

$$\overline{I} = \frac{1}{2\pi} \int_{-\infty}^{\infty} sG_2 \Delta^{-1} \exp(-rsf_1)\, dq \tag{49}$$

where

$$f_1 = iq \sin \phi + m_1 \cos \phi \, . \tag{50}$$

The method of steepest descents requires that

$$\frac{\partial f_1}{\partial q} = i \sin \phi + \frac{\partial m_1}{\partial q} \cos \phi = 0 \tag{51}$$

and assuming that $\cos \phi \neq 0$, which excludes the surface response, we obtain

$$\frac{\partial m_1}{\partial q} + i \tan \phi = 0 \, . \tag{52}$$

A value of q that satisfies this equation is a saddle point q_1, and the integral can be approximated in the vicinity of this point to yield

$$\overline{I} \simeq (2\pi rs)^{-1/2}(sG_2\Delta^{-1})|f_1''|^{-1/2} \exp(-rsf_1)|_{q=q_1} \tag{53}$$

where

$$f_1'' = \frac{\partial^2 f_1}{\partial q^2} = \frac{\partial^2 m_1}{\partial q^2} \cos\phi \neq 0 . \tag{54}$$

This approximation to the integral is valid as long as the saddle point is not on a branch cut. The calculational procedure to obtain $\partial^2 m/\partial q^2$ is given in Appendix B.

To invert into the time domain, we first substitute (see Fig. 3)

$$m_1 = \beta^{-1} \cos\alpha_1 \quad , \quad q_1 = -i\beta^{-1} \sin\alpha_1 \tag{55}$$

into equation (50) to obtain from equation (53)

$$\overline{I} \simeq (2\pi rs)^{-1/2}(sG_2\Delta^{-1})|f_1''|^{-1/2} \exp[-s(x \sin\alpha_1 + y \cos\alpha_1)/\beta] . \tag{56}$$

We then expand the slowness in powers of s (Appendix C)

$$1/\beta \simeq 1/\beta_1 + \zeta_1 s^2/\beta_1^2 \tag{57}$$

and use the convolution theorem to invert the transform. The final results are

$$u(x, y, \tau)/P = \frac{1}{\pi(2r)^{1/2}} \mathrm{Re}\left[\lim_{s\to 0}\left(\frac{sG_2}{\Delta}\right)\frac{1}{\chi_1 |f_1''|^{1/2}}\bigg|_{q=q_1} \times \int_0^\tau p^{-1/2}\mathrm{Ai}(\pm\delta_1)dp - \lim_{s\to 0}\left(\frac{sG_1}{\Delta}\right)\frac{1}{\chi_2 |f_2''|^{1/2}}\bigg|_{q=q_2} \times \int_0^\tau p^{-1/2}\mathrm{Ai}(\pm\delta_2)dp\right] \tag{58}$$

where

$$\chi_j = \left[3|\zeta_j|(x \sin\alpha_j + y\cos\alpha_j)/\beta_j^2\right]^{1/3} \tag{59}$$

$$\delta_j = \left[\tau - p - (x\sin\alpha_j + y\cos\alpha_j)/\beta_j\right]/\chi_j \tag{60}$$

in which $j = 1, 2$, and the positive sign in the argument of the Airy function is used if ζ_j is positive; otherwise the negative sign is used. Expressions for the v displacement are obtained by inserting D_1 in the first term of equation (58) and D_2 in the second according to equation (34).

Figure 6 shows the locations of the saddle points that correspond to the slowness surface in Fig. 2. The quasi-dilatational branch (m_1) has only one saddle point and it is always regular because it does not fall on a branch cut for $0 < \phi < \pi/2$. If $0 < \phi < \phi_2$, where ϕ_2 is the value of ϕ at point 2 in Fig. 6, the quasi-equivoluminal branch (m_2) has only one saddle point and it is regular. For $\phi_2 < \phi < \phi_4$, the m_2 branch has three saddle points labelled a, b, and c. One or two of these saddle points are irregular, because they

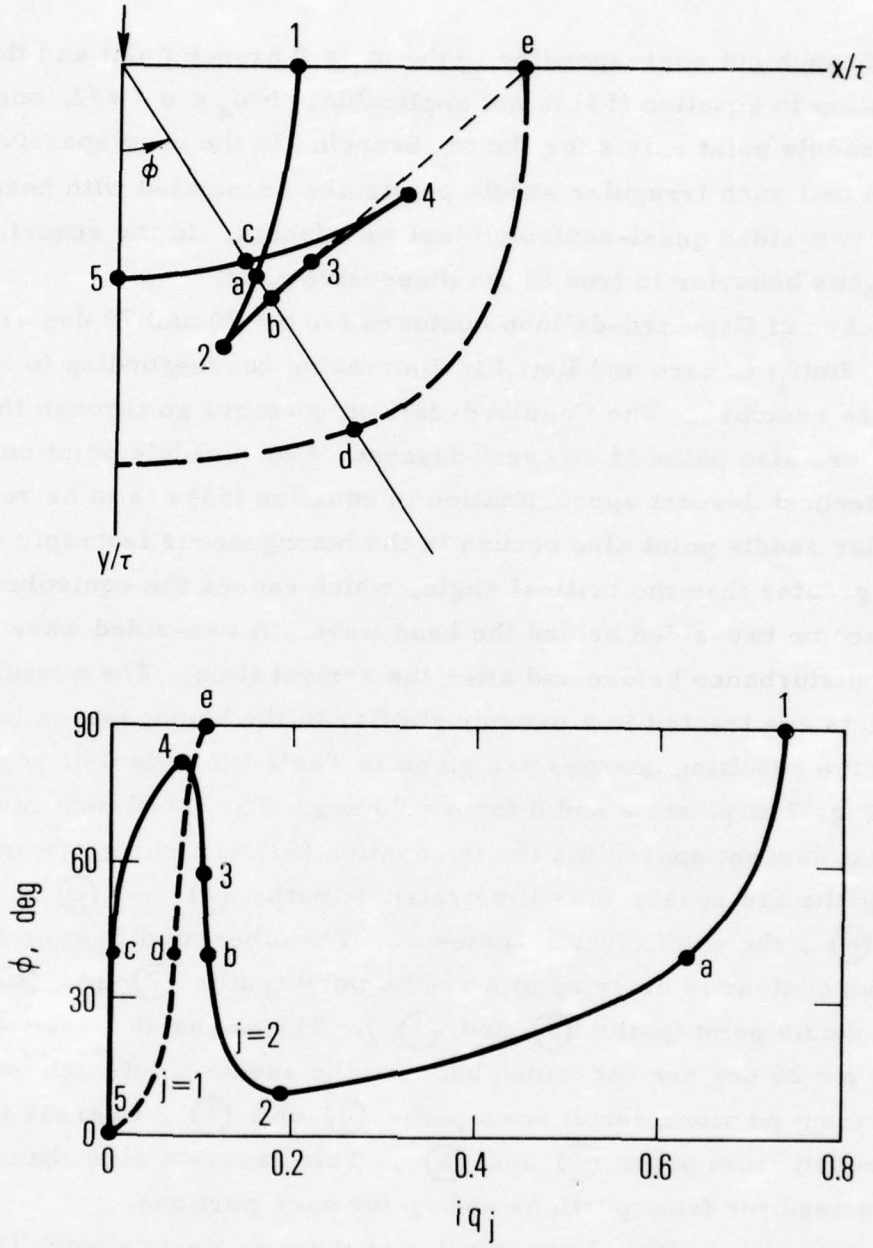

Figure 6. Correspondence of Saddle Points and Events

lie on the branch cut corresponding to the $m_1 = 0$ branch point and the approximation in equation (53) is not applicable. If $\phi_4 < \phi < \pi/2$, one irregular saddle point exists for the m_2 branch. In the nondispersive case, it is known that such irregular saddle points are associated with head wavefronts and two-sided quasi-equivoluminal wavefronts. In the sequel, we show that analogous behavior is true in the dispersive case.

Sketches of Cagniard-deHoop contours for $\phi = 20$ and 70 deg are shown in Fig. 7. $\mathrm{Im}(f_j)$ is zero and $\mathrm{Re}(f_j)$ is increasing corresponding to increasing τ/r on these contours. The Cagniard-deHoop contours go through the saddle points and are also paths of steepest descent. For a saddle point on a branch cut, the steepest descent approximation in equation (53) has to be rederived. An irregular saddle point also occurs in the homogeneous isotropic case [8] when ϕ is greater than the critical angle, which causes the equivoluminal wave to become two-sided behind the head wave. A two-sided wave is a wave that has a disturbance before and after the arrival time. The present irregular saddle points are treated in a manner similar to the homogeneous isotropic case, and the resulting changes are given in Table I for the four possibilities shown in Fig. 7 at points a and b for $\phi = 20$ deg. The coefficient in front of the steepest descent approximation in equation (53) will change from 1 to -1 when the paths are reversed as illustrated by paths ① and ② . On paths ③ and ④ , the coefficient becomes -i. The other modification involves whether the contour is arriving at a saddle point (paths ② and ④) or leaving a saddle point (paths ① and ③). The waves at these two saddle points for $\phi = 20$ deg are two-sided because the saddle points are on a branch cut. The front portions result from paths ② and ④ , whereas the back portions result from paths ① and ③ . This causes a sign change in δ_j, where p is used for front portions and -p for back portions.

The contours in Fig. 7 are similar to those in Kraut's work [2]. Crossing of the branch cut emanating from the $m_1 = m_2$ branch point is done by going on to the next Riemann sheet of the function. It is unnecessary to show paths going up along the cut, circling the branch point, and coming back down since the two resulting integrals are of opposite sign and therefore cancel.

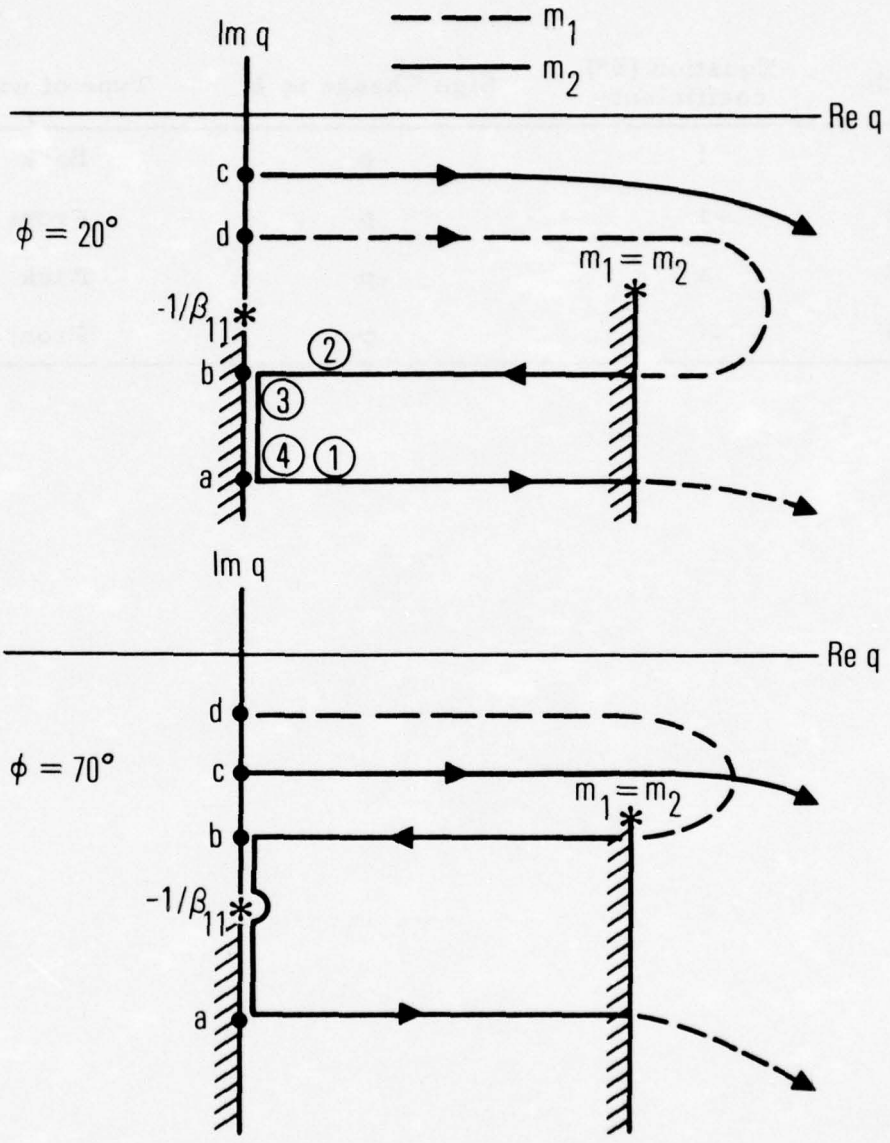

Figure 7. Sketch of Cagniard-deHoop Contours

Table I. Coefficients and Sign Changes in the Steepest Descent Approximation for the Quasi-Equivoluminal Two-Sided Wavefronts

Path	Equation (53) coefficient	Sign Change in δ_j	Type of wave
1	1	-p	Back
2	-1	p	Front
3	-i	-p	Back
4	-i	p	Front

The six separate contributions to the vertical displacement v for $\tau = 5$ and $\phi = 45$ deg are shown in Figs. 8-13. The nondispersive solution (dashed curve) is included for comparison. These solutions would partially overlap because the arrival times are close together; however, they are presented separately in order to emphasize the difference in amplitudes (note that the vertical scale factors are different) and to illustrate the effects of geometrical dispersion on the separate contributions. The effect of dispersion is particularly dramatic in Figs. 12 and 13, where the two-sided wave that corresponds to saddle point a is practically eliminated. This two-sided wave at point a is quasi-equivoluminal and is traveling in a direction that corresponds to $\alpha_2 \simeq 76$ deg which is almost parallel to the laminations. Previous investigations [4, 5] revealed that these shear-like waves traveling parallel to the layering are highly dispersive.

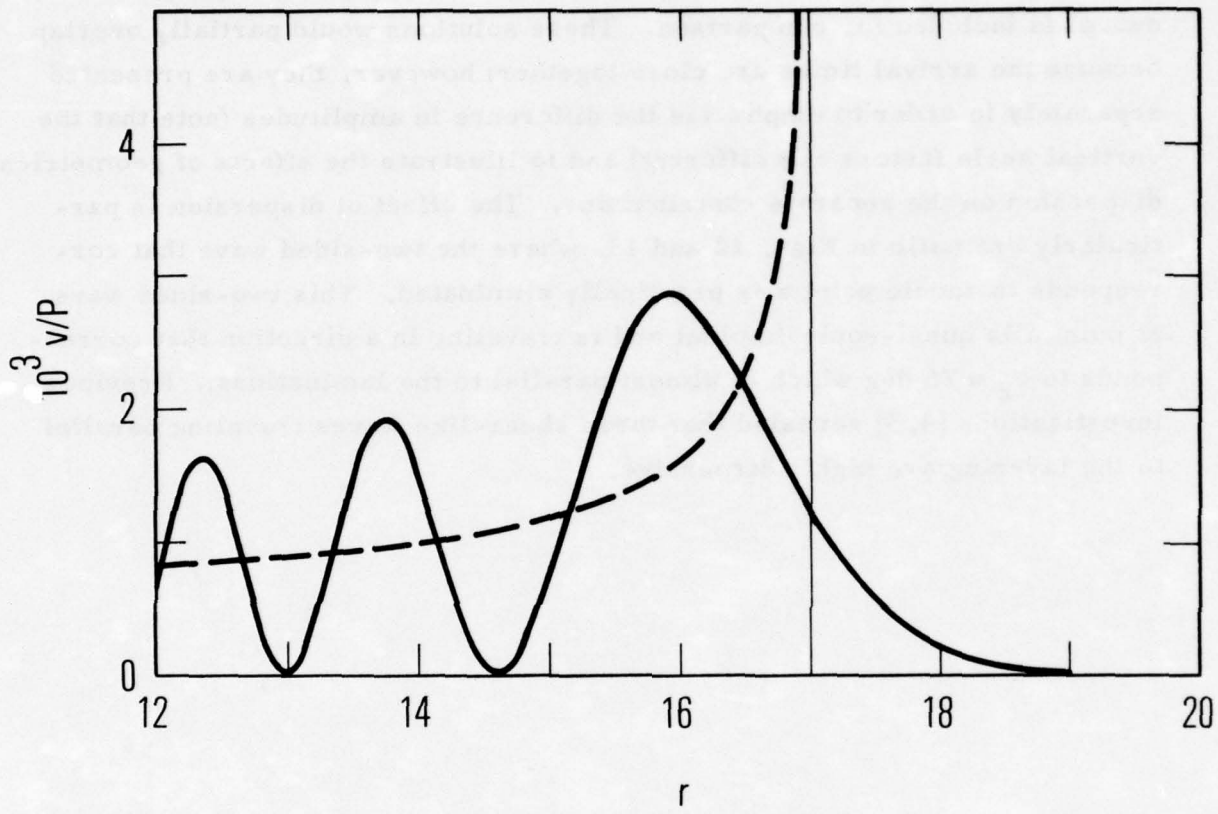

Figure 8. Vertical Displacement Due to Quasi-Dilational Wave Corresponding to Saddle Point d

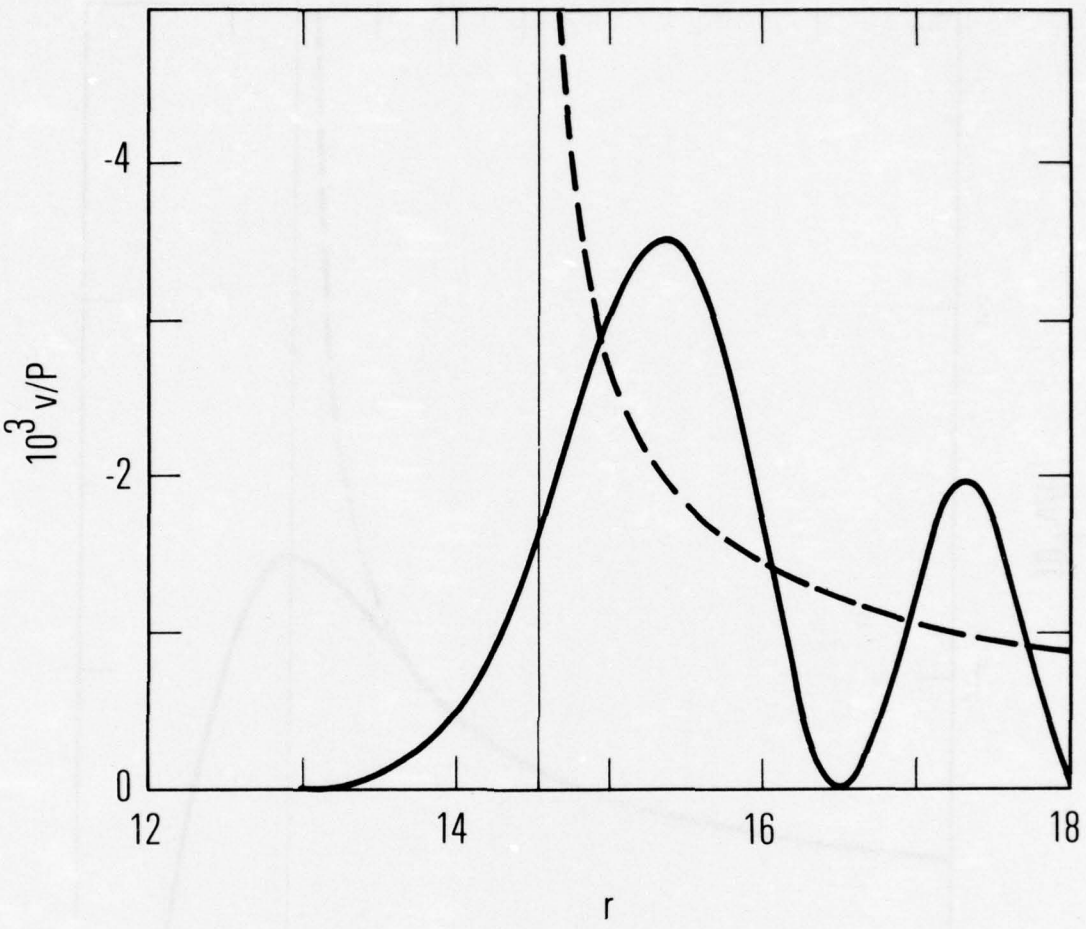

Figure 9. Vertical Displacement Due to Two-Sided Quasi-Equivoluminal Wave Corresponding to Saddle Point b; Front Part

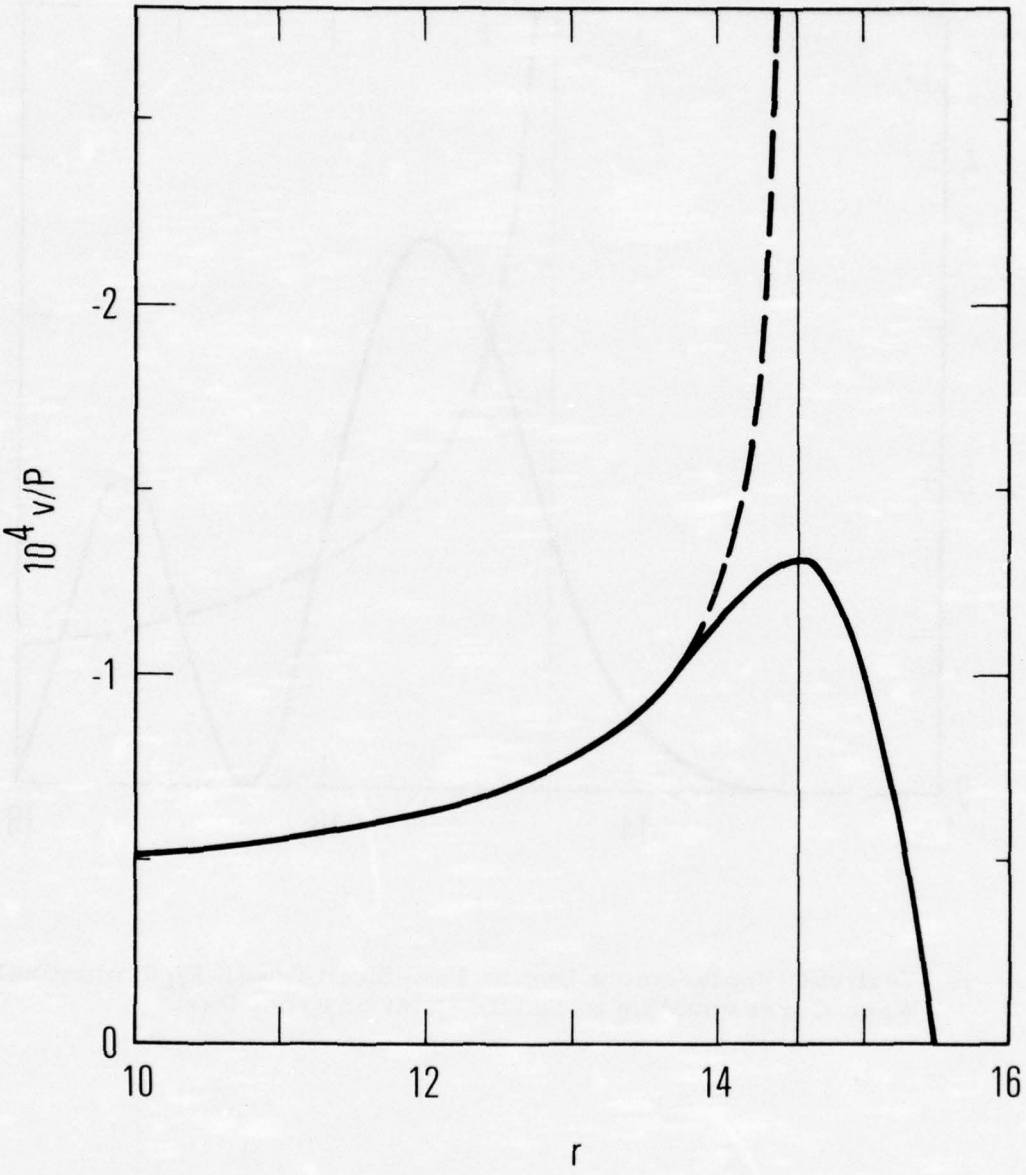

Figure 10. Vertical Displacement Due to Two-Sided Quasi-Equivoluminal Wave Corresponding to Saddle Point b; Back Part

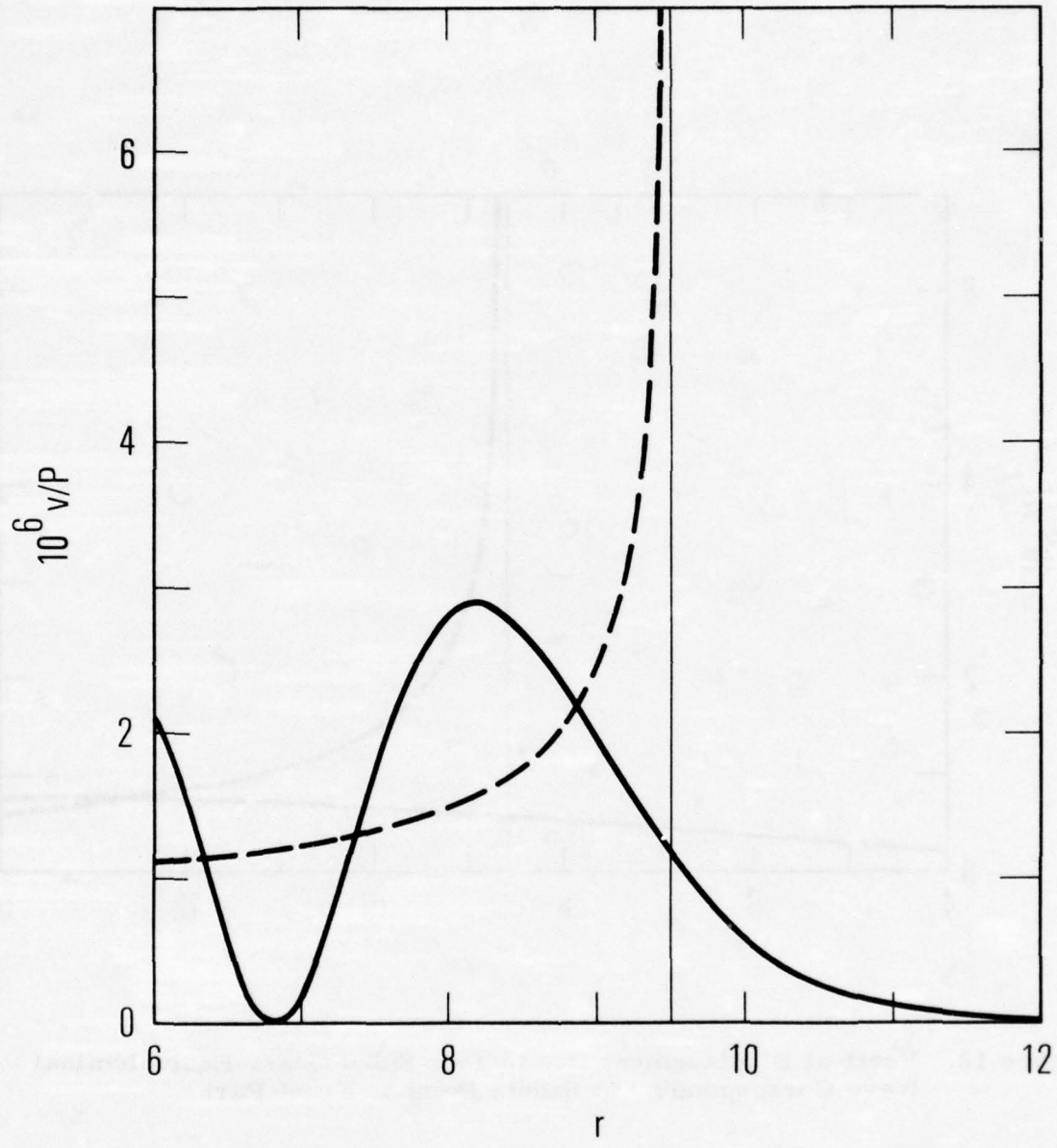

Figure 11. Vertical Displacement Due to Quasi-Equivoluminal Wave Corresponding to Saddle Point c

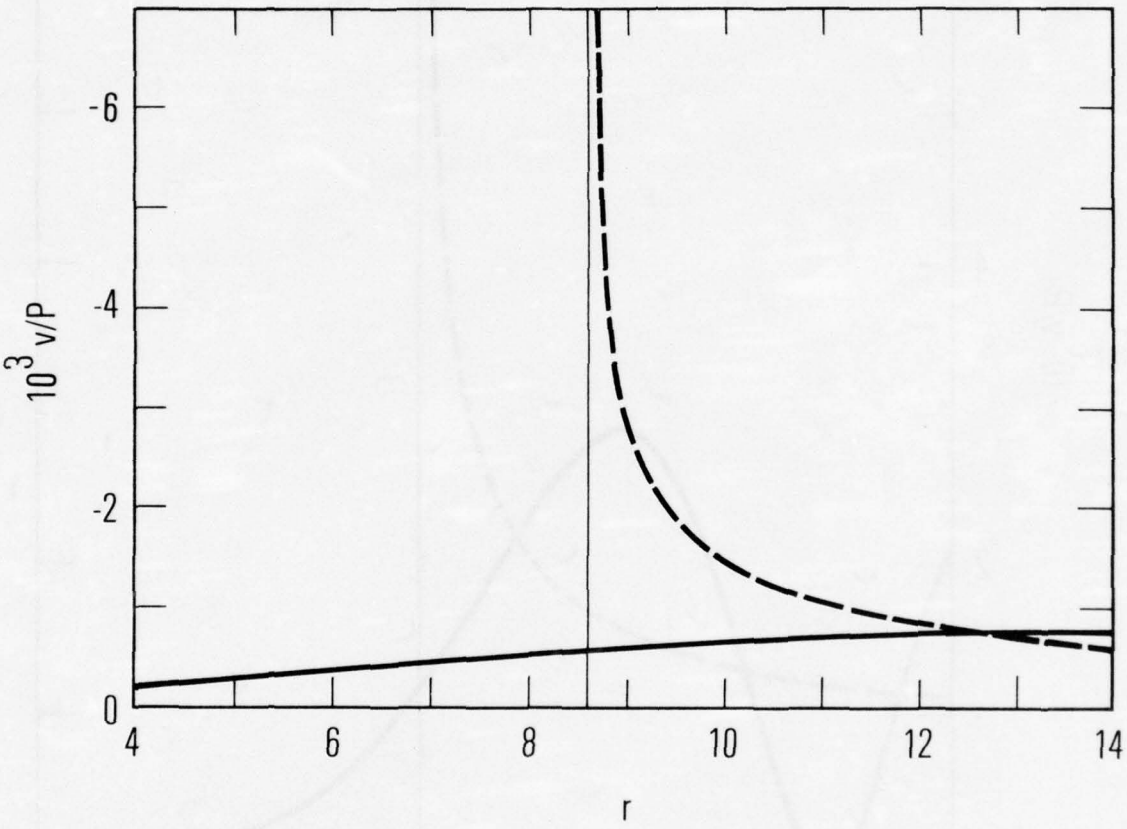

Figure 12. Vertical Displacement Due to Two-Sided Quasi-Equivoluminal Wave Corresponding to Saddle Point a; Front Part

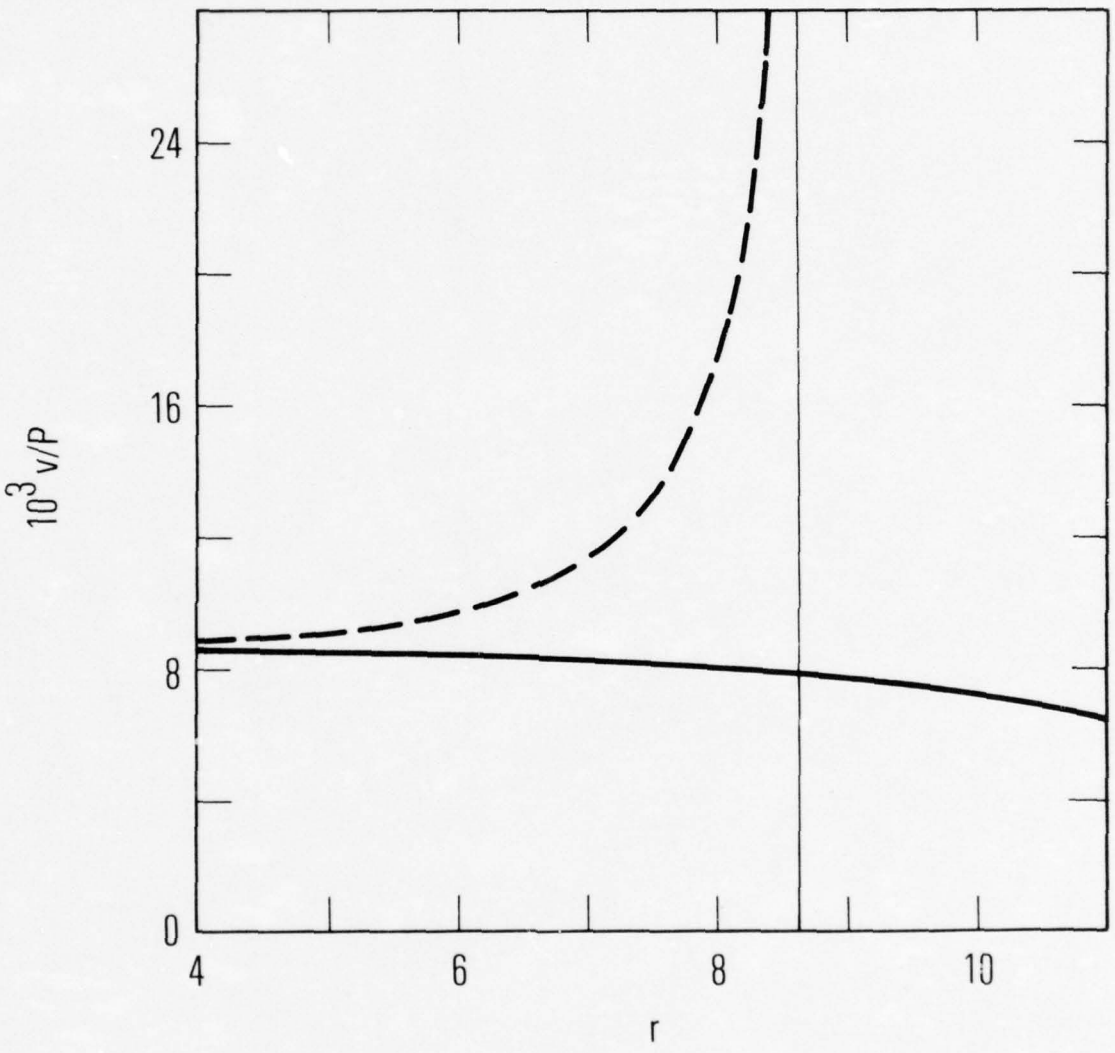

Figure 13. Vertical Displacement Due to Two-Sided Quasi-Equivoluminal Wave Corresponding to Saddle Point a; Back Part

V. HEAD WAVE CONTRIBUTION

The head wave is a reflected quasi-equivoluminal wave generated by the grazing incidence of the quasi-dilatational wave with the free surface. It consists of a planar wave that joins points 3 and e in Fig. 6. The head wave is tangent to the quasi-equivoluminal wave at point 3 and its nondispersive solution behaves as $O(|\tau - \tau^*|^{1/2})$ for $\phi_3 < \phi < \pi/2$, which is rather weak compared with the body wave singularities. The contour for $\phi = 70$ deg is shown in Fig. 7; the contour passes by the branch point located at $\mathrm{Im}(q) = -1/\beta_{11}$. The portion of the contour that is on the branch cut just below the branch point corresponds to the region just after the arrival of the head wave.

In order to estimate the effect of dispersion on the head wave, we begin with

$$\bar{u}(x, y, s)/P = -\frac{1}{2\pi}\int_{-\infty}^{\infty} sG_1\Delta^{-1} \exp(-rsf_2)\, dq \tag{61}$$

and expand f_2 down the imaginary axis near the branch point as (cf. Fig. 6.5, [8])

$$f_2(q) \simeq f_2(-i/\beta_{11}) + (q + i/\beta_{11})\, f_2'\Big|_{q = -i/\beta_{11}} = (\tau_{ds} + z)/r \tag{62}$$

where

$$\tau_{ds}/r = (1/\beta_{11}) \sin\phi_c + m_2\Big|_{q = -i/\beta_{11}}^{\cos\phi_c} \tag{63}$$

and since f_2 is positive and increasing on a path of steepest descent

$$z/r = \rho \left| f_2' \right|_{q = -i/\beta_{11}} , \qquad \rho = iq - 1/\beta_{11} . \tag{64}$$

Angles with subscript c denote critical angles and correspond to point 3 in Fig. 6. Note that since

$$\beta/\beta_{11} = \sin \alpha_c , \qquad \beta m_2 \Big|_{q = -i/\beta_{11}} = \cos \alpha_c \tag{65}$$

we can reduce τ_{ds} to

$$\tau_{ds} = (x \sin \alpha_c + y \cos \alpha_c)/\beta. \tag{66}$$

The branch function is found to have the form

$$m_1 \simeq -i\hat{m}_1 (\rho)^{1/2} \tag{67}$$

in the fourth quadrant just below the branch point, where $\hat{m}_1$ is a constant and G_1 is also of this form; thus, by including the contribution from the third quadrant, we obtain

$$\bar{u}(x,y,s)/P = \frac{Re}{\pi}\left(\frac{sG_1}{\Delta m_1}\right) \frac{\hat{m}_1}{|rf_2'|^{3/2}} \Bigg|_{q = -i/\beta_{11}} e^{-s\tau_{ds}} \int_0^\infty z^{1/2} \exp(-sz)\, dz . \tag{68}$$

The integral can be evaluated and the transform inverted to yield the long-time result

$$u(x, y, \tau)/P = \frac{Re}{\pi} \left[\lim_{s \to 0} \left(\frac{sG_1}{\Delta m_1} \right) \frac{\hat{m}_1 \, (\tau - \tau_{ds})^{1/2}}{\left| r f_2' \right|^{3/2}} \right| H(\tau - \tau_{ds}) \Bigg|_{q = -i/\beta_{11}} \Bigg] \tag{69}$$

for the nondispersive case. A convolution then provides the dispersive solution and the u displacement becomes

$$u(x, y, \tau)/P = \frac{1}{\pi r^{3/2}} \, Re \left[\lim_{s \to 0} \left(\frac{sG_1}{\Delta m_1} \right) \frac{\hat{m}_1}{\chi_2 \left| f_2' \right|^{3/2}} \right| \int_o^{\tau} p^{1/2} \, Ai \, (\pm \xi_2) \, dp \Bigg|_{q = -i/\beta_{11}} \Bigg] \tag{70}$$

where χ_2 and δ_2 are defined in equations (59) and (60). In order to obtain the expression for v, G_1 is replaced by $G_1 D_2$. These displacements decrease as $r^{-3/2}$, whereas the body waves decrease as $r^{-1/2}$. Also, the nondispersive head wave is smooth at its wavefront, and the convolution smooths it further. This solution is not applicable when $f_2' = 0$ at point 3, where the head wave becomes tangent to the quasi-equivoluminal wave.

VI. RAYLEIGH WAVE CONTRIBUTION

The largest contribution on the surface in the far field is due to the Rayleigh wave. When y is zero, the Cagniard contours encounter the Rayleigh pole located as shown in Fig. 5, and by approximating the integrals in the vicinity of the pole, it is possible to determine the nature and strength of the Rayleigh wave singularity for the nondispersive case. A low-frequency expansion and a convolution then yields the dispersive solution as in the previous sections for the body waves and head wave.

The Rayleigh denominator is first expanded as

$$\Delta \simeq (q + i/\beta_R)\ \Delta' \Big|_{q\ =\ -i/\beta_R} . \tag{71}$$

The integrals are then approximated over small portions of the contour in the fourth quadrant along the imaginary q axis just above and below the pole. The first integral of equation (33) becomes the Cauchy principal value

$$\overline{I} = \lim_{\epsilon \to o} \left[\int_{-i/\beta_R\ +\ i\epsilon}^{-i/\beta_R} \frac{e^{-isxq}}{q + i/\beta_R}\, dq + \int_{-i/\beta_R}^{-i/\beta_R\ -\ i\epsilon} \frac{e^{-isxq}}{q + i/\beta_R}\, dq \right] \frac{sG_2}{2\pi\Delta'} \Bigg|_{q\ =\ -i/\beta_R} . \tag{72}$$

Substitution of

$$\tau = iqx \tag{73}$$

and completion of the resulting integral yields

$$\overline{I} = \frac{1}{2\pi}\left[\text{P. V.}\int_0^\infty \frac{e^{-s\tau}}{\tau - x/\beta_R}\, d\tau \left(\frac{sG_2}{\Delta'}\right)\bigg|_{q\,=\,-i/\beta_R}\right]. \tag{74}$$

The long-time result is then obtained by inspection as

$$I = \frac{1}{2\pi}\lim_{s\to o}\left.\frac{sG_2}{(\tau - x/\beta_R)\,\Delta'}\right|_{q\,=\,-i/\beta_R} \tag{75}$$

The integrals are also evaluated in the third quadrant, and the conjugate properties of the integrals are used to reduce the far-field nondispersive results to

$$u(x, 0, \tau)/P = \frac{1}{\pi}\,\text{Re}\left[\lim_{s\,\to\,0}\left.\frac{s\,(G_2 - G_1)}{\Delta'}\right|_{q\,=\,-i/\beta_{R0}}\frac{1}{\tau - x/\beta_{R0}}\right] = 0 \tag{76}$$

$$v(x, 0, \tau)/P = \frac{1}{\pi}\,\text{Re}\left[\lim_{s\,\to\,0}\left.\frac{s\,(G_2D_1 - G_1D_2)}{\Delta'}\right|_{q\,=\,-i/\beta_{R0}}\frac{1}{\tau - x/\beta_{R0}}\right] \tag{77}$$

where the nondispersive Rayleigh wave velocity is given by

$$\beta_{R0} = \beta_R\Big|_{s\,=\,0}. \tag{78}$$

Note that u is zero since the quantity in brackets in equation (76) is found to be imaginary for the parameters selected in this investigation. However, the Rayleigh pole also adds a residue term to the solution for u, and this can be evaluated by considering a small circular contour around the pole to yield

$$u(x, 0, \tau)/P = \mathrm{Re}\left[\lim_{s\to 0} \frac{is\,(G_1 - G_2)}{\Delta'}\bigg|_{q = -i/\beta_{R0}} \delta(\tau - x/\beta_{R0})\right]. \tag{79}$$

An analytical expression for the derivative of Δ with respect to q is given in Appendix D.

The dispersive solution corresponding to equation (77) is developed by expanding the Rayleigh wave velocity as

$$1/\beta_R \simeq 1/\beta_{R0} + \zeta_R s^2/\beta_{R0}^2 \tag{80}$$

and using the convolution theorem to yield

$$v(x, 0, \tau)/P = \frac{1}{\pi}\,\mathrm{Re}\left\{\lim_{s\to 0} \frac{s\,(G_2D_1 - G_1D_2)}{\Delta'} \frac{1}{\chi_R}\int_0^\tau p^{-1}\left[\mathrm{Ai}\left(\frac{\tau - p - x/\beta_{R0}}{\chi_R}\right) - \mathrm{Ai}\left(\frac{\tau + p - x/\beta_{R0}}{\chi_R}\right)\right] dp\right\} \tag{81}$$

where

$$\chi_R = \left(3|\zeta_R|\,x/\beta_{R0}^2\right)^{1/3}. \tag{82}$$

The appropriate dispersive solution for the residue term is easily verified to be

$$u(x, 0, \tau)/P = \mathrm{Re}\left[\lim_{s \to 0} \frac{is\,(G_1 - G_2)}{\Delta' \chi_R}\bigg|_{q = -i/\beta_{R0}} \mathrm{Ai}\left(\frac{\tau - x/\beta_{R0}}{\chi_R}\right)\right]. \quad (83)$$

Numerical results for the vertical displacement on the surface [equations (77) and (81)] are shown in Fig. 14 for the same parameters as the previous figures. The value of ζ_R in equation (80) for the expansion of the Raylieigh wave velocity was determined to be approximately 1.03 by fitting a parabola through s = 0 and each of the points s = 0.01, 0.02 and 0.03. This yielded three values for ζ_R that were then used to find ζ_R at s = 0 by extrapolation with another parabola. Note from Fig. 14 that the dispersion eliminates the Rayleigh wave singularity and alters the entire shape of the response curve. Similar results are shown in Fig. 15 for ζ_R = 0.08 corresponding to γ = 10.

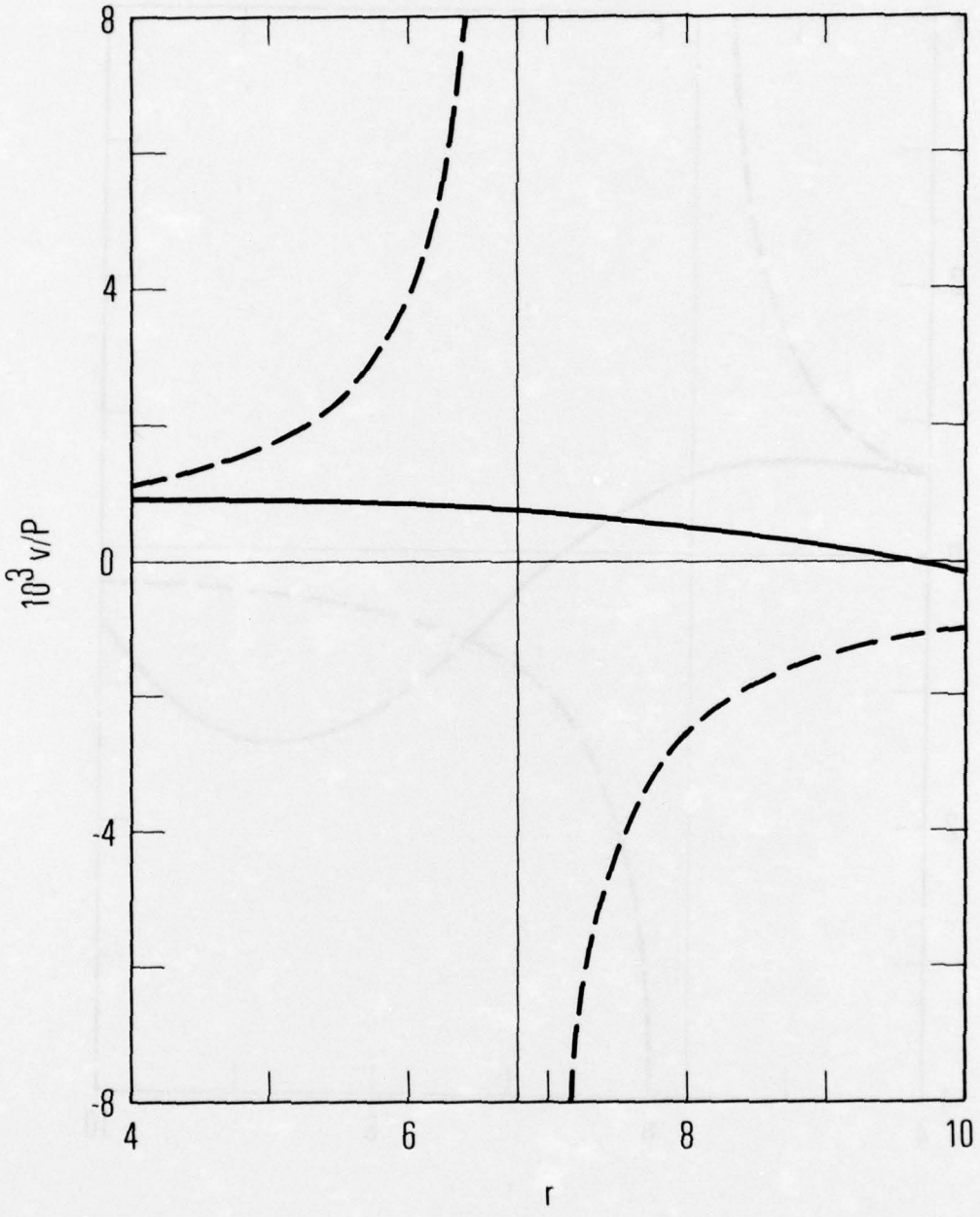

Figure 14. Vertical Displacement Due to Rayleigh Surface Wave (γ = 100)

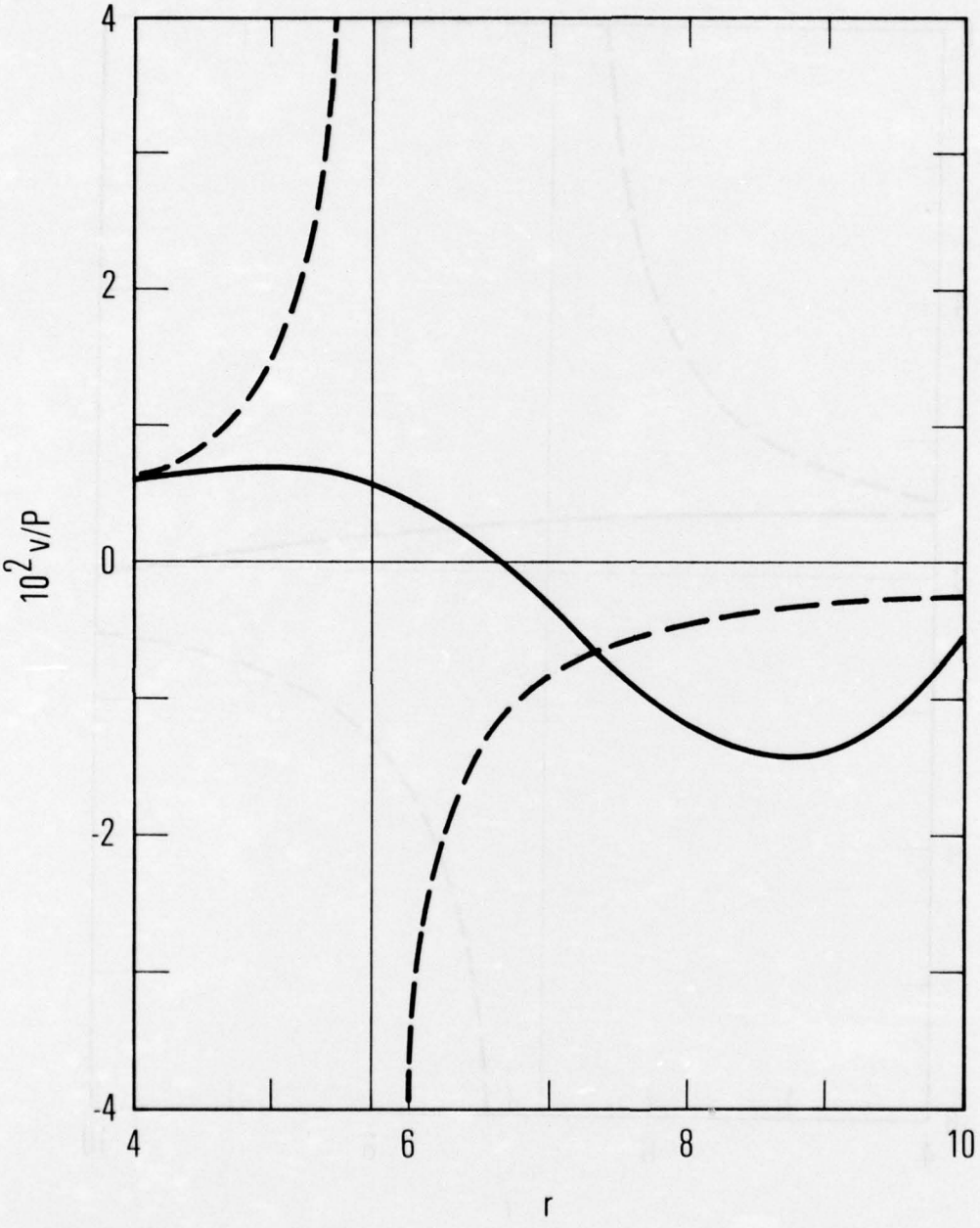

Figure 15. Vertical Displacement Due to Rayleigh Surface Wave ($\gamma = 10$)

VII. CONCLUSIONS

An approximate far-field solution has been presented for the response of a periodically laminated composite half space subjected to a line impulse. The governing equations were from the effective stiffness theory [4]. The solution consists of convolution integrals that arise when the phase velocities are expanded for low frequency. As the dispersion caused by the laminations is allowed to approach zero, the solution reduces to the wavefront expansions for the corresponding homogeneous transversely isotropic half space.

Numerical results were presented that illustrate the effect of dispersion on the body waves and the Rayleigh surface wave. In each case, the wavefront singularities are eliminated by the dispersion, and the displacements become continuous.

REFERENCES

1 Lamb, H., "On the Propagation of Tremors Over the Surface of an Elastic Solid," Philosophical Transactions of the Royal Society of London, Series A, Mathematical and Physical Sciences, Vol. 203, 1904, pp. 1-42.

2 Kraut, E. A., "Propagation of a Pulse from a Surface Line Source on a Transversely Isotropic Half Space," Ph. D. Thesis, University of California, Los Angeles, 1962.

3 Kraut, E. A., "Advances in the Theory of Anisotropic Elastic Wave Propagation," Reviews of Geophysics, Vol. 1, No. 3, pp. 401-448, Aug. 1963.

4 Sun, C. T., Achenbach, J. D., and Herrmann, G., "Continuum Theory for a Laminated Medium," Journal of Applied Mechanics, Vol. 35, No. 3, Trans. ASME, Vol. 90, Series E, Sept. 1968, pp. 467-475.

5 Sve, C., and Whittier, J. S., "One-Dimensional Pulse Propagation in an Obliquely Laminated Half Space," Journal of Applied Mechanics, Vol. 37, No. 3, Trans. ASME, Vol. 92, Series E., Sept. 1970, pp. 778-782.

6 Sve, C., and Herrmann, G., "Moving Load on a Laminated Composite," Journal of Applied Mechanics, Vol. 41, No. 3, Trans. ASME, Vol. 96, Series E, Sept. 1974, pp. 663-667.

7 Sun, C. T. "Surface Waves in Layered Media," Bulletin of the Seismological Society of America, Vol. 60, No. 2, April, 1970, pp. 345-366.

8 Miklowitz, J., Theory of Elastic Waves and Waveguides, North-Holland Publishing Company, Amsterdam, 1977, Chaps. 5, 6.

APPENDIX A. DERIVATIVES FOR WAVE SURFACE

The derivatives required to locate the nondispersive (s = 0) wave surface are

$$\frac{\partial \Phi_0}{\partial m} = 4B_1B_4m^3 - 2m\left(B_2B_4 + B_1B_5 - B_3^2\right)\Big|_{s=0} \tag{84}$$

$$\frac{\partial \Phi_0}{\partial q} = \left(2B_3B_3' - B_2'B_4 - B_1B_5'\right)m^2 + B_2'B_5 + B_2B_5'\Big|_{s=0} \tag{85}$$

where the primes represent partial differentiation with respect to q. The derivatives of the B's for s = 0 simplify to

$$\begin{aligned} B_2'\Big|_{s=0} &= A_2' - 2A_5A_5'/A_{11}\Big|_{s=0} \\ B_3'\Big|_{s=0} &= A_3' + A_5'A_9/A_{11} + A_8'A_4/A_{10}\Big|_{s=0} \\ B_5'\Big|_{s=0} &= A_7' - 2A_8A_8'/A_{10}\Big|_{s=0} \end{aligned} \tag{86}$$

where

$$\begin{aligned} A_2' &= 2q[\eta\gamma\delta_f + (1 - \eta)\,\delta_m] \\ A_3' &= \epsilon_m + 1 \quad , \quad A_5' = \eta(\epsilon_f\gamma - \epsilon_m) \\ A_7' &= 2q(\eta\gamma + 1 - \eta) \quad , \quad A_8' = \eta(\gamma - 1) \quad . \end{aligned} \tag{87}$$

APPENDIX B. SECOND DERIVATIVE AT A SADDLE POINT

In order to determine $\partial^2 m/\partial q^2$ at a saddle point, we begin with

$$\Phi_0(m, q) = 0. \tag{88}$$

Implicit differentiation yields

$$\Phi_{0,q} + \Phi_{0,m} m_{,q} = 0 \tag{89}$$

and

$$\Phi_{0,qq} + 2\Phi_{0,mq} m_{,q} + \Phi_{0,mm} m_{,q}^2 + \Phi_{0,m} m_{,qq} = 0. \tag{90}$$

However, at a saddle point

$$m_{,q} = -i \tan \phi \tag{91}$$

leading to

$$m_{,qq} = (-\Phi_{0,qq} + 2i\Phi_{0,mq} \tan \phi + \Phi_{0,mm} \tan^2 \phi)/\Phi_{0,m} \tag{92}$$

where

$$\Phi_{0,mq} = 2m(2B_3B_3' - B_2'B_4 - B_1B_5')\Big|_{s=0} \tag{93}$$

$$\Phi_{0,mm} = 12m^2 B_1B_4 - 2(B_2B_4 + B_1B_5 - B_3^2)\Big|_{s=0} . \tag{94}$$

The remaining derivative $\Phi_{0,\,qq}$ is found by differentiating the determinant

$$\Phi_0 = \frac{1}{(A_{10}A_{11})}\Big|_{s=0} \begin{vmatrix} A_1m^2 - A_2 & -A_3m & A_4m & A_5 \\ A_3m & A_6m^2 - A_7 & -A_8 & A_9m \\ A_4m & A_8 & A_{10} & 0 \\ -A_5 & A_9m & 0 & A_{11} \end{vmatrix}_{s=0} = 0 \tag{95}$$

which yields a sum of 16 determinants

$$\Phi_{0,\,qq} = \frac{1}{(A_{10}A_{11})}\Big|_{s=0} \sum_{j=1}^{4}\sum_{k=1}^{4} \Phi_{0jk} \tag{96}$$

where Φ_{0jk} is Φ_0 with columns j and k replaced by their first derivatives. Note that $\Phi_{0jk} = \Phi_{0kj}$. When j = k, column j is replaced by its second derivative. Appendix A contains the first derivatives of the A's; the second derivatives are

$$A_2'' = 2[\eta\gamma\delta_f + (1 - \eta)\delta_m] \tag{97}$$

$$A_7'' = 2(\eta\gamma + 1 - \eta) \quad . \tag{98}$$

APPENDIX C. EXPANSION OF SLOWNESS IN POWERS OF s

The expansion for the slowness in equation (57) can be obtained by recognizing that

$$m_j = \cos \alpha_j \left(\frac{1}{\beta_j} + \frac{\zeta_j s^2}{\beta_j^2} \right) = \frac{\cos \alpha_j}{\beta_j} + \frac{m_{,ss}}{2} \Big|_{s=0} s^2 \tag{99}$$

and since

$$m_{,ss}|_{s=0} = -\Phi_{,ss} / \Phi_{,m}|_{s=0} \tag{100}$$

we find that

$$\zeta_j = \frac{-\beta_j^2}{2 \cos \alpha_j} \frac{\Phi_{,ss}}{\Phi_{,m}} \Big|_{\substack{s=0 \\ q=q_j}} . \tag{101}$$

These derivatives can be determined by evaluating

$$\Phi_{,m}|_{s=0} = 4B_1 B_4 m^3 - 2m(B_2 B_4 + B_1 B_5 - B_3^2)|_{s=0} \tag{102}$$

$$\Phi_{,ss}|_{s=0} = (B_4 B_{1,ss} + B_1 B_{4,ss}) m^4 - (B_2 B_{4,ss} + B_4 B_{2,ss}$$

$$+ B_1 B_{5,ss} + B_5 B_{1,ss} - 2B_3 B_{3,ss}) m^2 + B_5 B_{2,ss} + B_2 B_{5,ss}|_{s=0} \tag{103}$$

where

$$B_{1,ss}\big|_{s=0} = A_{1,ss} - 2A_4A_{4,ss}/A_{10} + A_4^2 A_{10,ss}/A_{10}^2\big|_{s=0}$$

$$B_{2,ss}\big|_{s=0} = A_5^2 A_{11,ss}/A_{11}^2\big|_{s=0}$$

$$B_{3,ss}\big|_{s=0} = A_5A_{9,ss}/A_{11} - A_5A_9A_{11,ss}/A_{11}^2$$

$$- A_4A_8A_{10,ss}/A_{10}^2 + A_8A_{4,ss}/A_{10}\big|_{s=0}$$

$$B_{4,ss}\big| = A_{6,ss} - 2A_9A_{9,ss}/A_{11} + A_9^2 A_{11,ss}/A_{11}^2\big|_{s=0}$$

$$B_{5,ss}\big|_{s=0} = A_8^2A_{10,ss}/A_{10}^2\big|_{s=0} \qquad (104)$$

and

$$A_{1,ss} = (1 + q^2\,\delta_m)\,(1 - \eta)/6 \quad , \quad A_{4,ss} = \eta A_{1,ss}$$

$$A_{6,ss} = (1 + q^2)\,(1 - \eta)/6 \quad , \quad A_{9,ss} = \eta\, A_{6,ss}$$

$$A_{10,ss} = \eta^2 A_2/6 \quad , \quad A_{11,ss} = \eta^2 A_7/6 \qquad (105)$$

APPENDIX D. RESIDUE TERM FOR RAYLEIGH POLE

The derivative in the denominator of equation (75) for small s is

$$\Delta' = G_1' H_2 + G_1 H_2' - G_2' H_1 - G_2 H_1' \tag{106}$$

where

$$G_j'/s = - iD_j - iqD_j' - m_j' - m_j' A_1 - A_4 E_j'/s$$

$$D_j' = (B_2' - 2B_1 m_j m_j')/im_j B_3$$

$$+ (B_2 - B_1 m_j^2)\,(im_j' B_3 + im_j B_3')/m_j^2 B_3^2$$

$$E_j'/s = (iA_8' D_j + i A_8 D_j' - m_j' A_4)/A_{10}$$

$$H_j'/s = - i \epsilon_m - m_j' D_j A_6 - m_j D_j' A_6 - A_9 F_j'/s$$

$$F_j'/s = (iA_5' - m_j' D_j A_9 - m_j D_j' A_9)/A_{11} \tag{107}$$

and

$$j = 1, 2.$$

THE IVAN A. GETTING LABORATORIES

The Laboratory Operations of The Aerospace Corporation is conducting experimental and theoretical investigations necessary for the evaluation and application of scientific advances to new military concepts and systems. Versatility and flexibility have been developed to a high degree by the laboratory personnel in dealing with the many problems encountered in the nation's rapidly developing space and missile systems. Expertise in the latest scientific developments is vital to the accomplishment of tasks related to these problems. The laboratories that contribute to this research are:

Aerophysics Laboratory: Launch and reentry aerodynamics, heat transfer, reentry physics, chemical kinetics, structural mechanics, flight dynamics, atmospheric pollution, and high-power gas lasers.

Chemistry and Physics Laboratory: Atmospheric reactions and atmospheric optics, chemical reactions in polluted atmospheres, chemical reactions of excited species in rocket plumes, chemical thermodynamics, plasma and laser-induced reactions, laser chemistry, propulsion chemistry, space vacuum and radiation effects on materials, lubrication and surface phenomena, photosensitive materials and sensors, high precision laser ranging, and the application of physics and chemistry to problems of law enforcement and biomedicine.

Electronics Research Laboratory: Electromagnetic theory, devices, and propagation phenomena, including plasma electromagnetics; quantum electronics, lasers, and electro-optics; communication sciences, applied electronics, semiconducting, superconducting, and crystal device physics, optical and acoustical imaging; atmospheric pollution; millimeter wave and far-infrared technology.

Materials Sciences Laboratory: Development of new materials; metal matrix composites and new forms of carbon; test and evaluation of graphite and ceramics in reentry; spacecraft materials and electronic components in nuclear weapons environment; application of fracture mechanics to stress corrosion and fatigue-induced fractures in structural metals.

Space Sciences Laboratory: Atmospheric and ionospheric physics, radiation from the atmosphere, density and composition of the atmosphere, aurorae and airglow; magnetospheric physics, cosmic rays, generation and propagation of plasma waves in the magnetosphere; solar physics, studies of solar magnetic fields; space astronomy, x-ray astronomy; the effects of nuclear explosions, magnetic storms, and solar activity on the earth's atmosphere, ionosphere, and magnetosphere; the effects of optical, electromagnetic, and particulate radiations in space on space systems.

THE AEROSPACE CORPORATION
El Segundo, California